# A New DC Current Detector Using Bridge-Connected Magnetic Circuit


doi: 10.1063/1.342254

# A new dc current detector using bridge-connected magnetic circuit

S. Okanuma
*Department of Electrical Engineering, Fukushima National College of Technology, Iwaki 970, Japan*
O. Ichinokura and K. Murakami
*Department of Electrical Engineering, Tohoku University, Sendai 980, Japan*

This paper describes performance characteristics of a bridge-connected magnetic circuit with single output winding in dc control. The difference between positive and negative amplitudes of output current changes with the dc control current. An application of the bridge-connected magnetic circuit to a dc current detector is presented in this paper.

## INTRODUCTION

The authors reported a bridge-connected magnetic circuit which is constructed with an amorphous toroidal core and a U-form core, and its applications to measuring and controlling devices.[1,2] In these applications, the output winding was wound separately around both sides of the toroidal core which is divided by the U-form core.

On the other hand, the output winding can be formed around one side of the toroidal core.[3] Few papers, however, have reported the detailed operation of the magnetic circuit with single output winding.

In this paper, we describe performance characteristics of a bridge-connected magnetic circuit in dc control. The difference between positive and negative amplitudes of output current changes by the dc current and its flow direction. Based on this feature, we present a new dc current detector.

## FUNDAMENTAL OPERATIONS

Figure 1(a) shows a core structure of bridge-connected magnetic circuit. In the figure, $A$ is an amorphous toroidal core with rectangular $B$-$H$ loop and $B$ is a U-form core with low permeability. Figure 1(b) shows the basic circuit where $N_L$ is the output winding, $N_C$ is the control winding, $e_P$ is the supply voltage, $i_L$ is the output current, and $I_C$ is the dc current.

For the analysis, let No. 1 and No. 2 denote the magnetic paths of the toroidal core which is divided by the U-form core, and $\phi_1$, $\phi_2$, and $\phi_3$ be the fluxes of No. 1, No. 2, and U-form core. The positive of the currents and fluxes are in the direction of the arrows shown in the figure.

Figure 2 shows the voltage, current, and fluxes waveforms. This shows that the positive amplitude of $i_L$ is larger than the negative one when $I_C$ flows in the positive direction, and that the negative amplitude of $i_L$ is larger than the positive one when $I_C$ flows in the negative direction.

Now, we obtain the output current under simple assumptions. Figure 3 shows the magnetization curves used for the analysis. In the figure, $\alpha$ is the magnetization curve of the toroidal core, where $P_r$ is the saturating permeance and $\Phi_S$ is the saturation flux. $\beta$ is the magnetization curve of U-form core, where $P_C$ is the permeance.

Let the supply voltage $e_P = \sqrt{2}E_P \sin \omega t$, and let the magnetic intensities of No. 1, No. 2, and U-form core be $H_1$, $H_2$, and $H_3$. Then the fundamental equations formed in Fig. 1(b) are

$$\phi_1 - \phi_2 + \phi_3 = 0, \tag{1}$$

$$H_1 l_L + H_2 l_L = N_L i_L, \tag{2}$$

$$H_2 l_L + H_3 l_C = N_L i_L + N_C I_C, \tag{3}$$

$$N_L \left(\frac{d\phi_2}{dt}\right) + R i_L = \sqrt{2}E_P \sin \omega t, \tag{4}$$

where $l_L$ is the length of the magnetic paths No. 1 and No. 2, and $l_C$ is that of U-form core.

Figure 4 shows the time variations of voltage, current, and fluxes when $I_C$ flows in the positive direction. In the figure, $t_1$, $t_2$, $t_3$, and $t_4$ are the times. $I_{Lp}$ is the positive amplitude of $i_L$ and $I_{Ln}$ the negative one.

### A. Mode I ($t_2 \leqslant t < t_1$)

In this mode, $H_1 = H_2 = 0$ because No. 1 and No. 2 are not saturated. So, $i_L = 0$. The flux $\phi_2$ is obtained by using

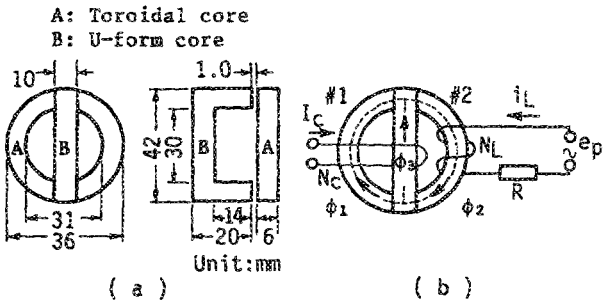


FIG. 1. Schematic diagram of the birdge-connected magnetic circuit. (a) Core structure. (b) Basic circuit.

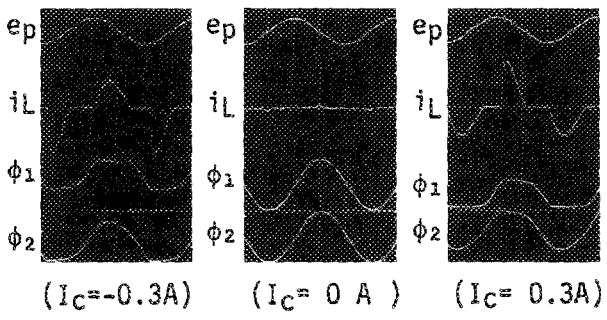


FIG. 2. Observed waveforms obtained in the circuit shown in Fig. 1(b).

 0021-8979/88/225702-03$02.40  

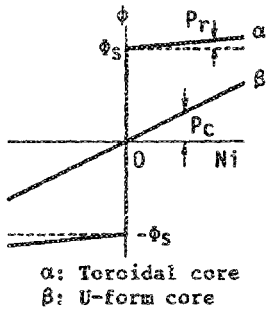


FIG. 3. Assumptions of the magnetization curves of the cores.

Eqs. (1) and (4) under the initial condition that $\phi_1 = -\Phi_S$ at $t = t_1$. That is,

$$\phi_2 = \phi_P(\cos \omega t_1 - \cos \omega t) - \Phi_S + P_C N_C I_C, \qquad (5)$$

where $\phi_P = \sqrt{2}E_P/\omega N_L$. When $\phi_2$ reaches to $\Phi_S$, the current $i_L$ begins to flow and the core operation turns in next mode.

### B. Mode II ($t_2 < t < t_3$)

In this mode, No. 2 is saturated. The permeance of the saturated magnetic path No. 2 is $2P_r$. Then

$$\frac{d\phi_2}{dt} = 2P_r N_L\left(\frac{di_L}{dt}\right).$$

Therefore, the circuit equation is obtained by using Eq. (4), as follows:

$$2P_r N_L{}^2\left(\frac{di_L}{dt}\right) + Ri_L = \sqrt{2}E_P \sin \omega t. \qquad (6)$$

From Eq. (6), we obtain $i_L$ under the initial condition that $i_L = 0$ at $t = t_2$. That is,

$$i_L = \left(\frac{\sqrt{2}E_P}{Z_r}\right)\left[\sin(\omega t - \xi_r) - \sin(\omega t_2 - \xi r)\exp\left(\frac{t_2 - t}{\tau_r}\right)\right], \qquad (7)$$

where $\tau_r = 2P_r N_L^2/R$, $\xi_r = \arctan(\omega\tau_r)$, and $Z_r = R\sqrt{1 + (\omega\tau_r)^2}$.

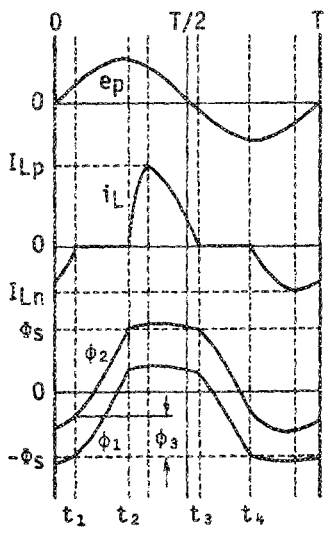


FIG. 4. Time variations of the voltage, current, and fluxes.

When $i_L$ given by Eq. (7) decreases to zero, No. 2 turns in unsaturated region and the operation turns in the next mode.

### C. Mode III ($t_3 < t < t_4$)

In this mode, No. 1 and No. 2 are not saturated. So, $i_L = 0$. $\phi_1$ is obtained by usig Eqs. (1) and (4) under the initial condition that $\phi_2 = \Phi_S$ at $t = t_3$.

$$\phi_1 = \phi_P(\cos \omega t_3 - \cos \omega t) + \Phi_S - P_C N_C I_C. \qquad (8)$$

When $\phi_1$ reaches to $-\Phi_S$, the output current $i_L$ begins to flow and the operation turns in the next.

### D. Mode IV ($t_4 < t < t_1 + T$)

In this mode, No. 1 is saturated:

$$\frac{d\phi_2}{dt} = (2P_r + P_C)N_L\left(\frac{di_L}{dt}\right).$$

The circuit equation is

$$(2P_r + P_C)N_L{}^2\left(\frac{di_L}{dt}\right) + Ri_L = \sqrt{2}E_P \sin \omega t. \qquad (9)$$

From Eq. (9), we obtained the current $i_L$ under the initial condition that $i_L = 0$ at $t = t_4$.

$$i_L = \left(\frac{\sqrt{2}EP}{Z_{Cr}}\right)\left[\sin(\omega t - \xi_{Cr}) - \sin(\omega t_4 - \xi_{Cr})\exp\left(\frac{t_4 - t}{\tau_{Cr}}\right)\right], \qquad (10)$$

where $\tau_{Cr} = (2P_r + P_C)N_L^2/R$, $\xi_{Cr} = \arctan(\omega\tau_{Cr})$, and $Z_{Cr} = R\sqrt{1 + (\omega\tau_{Cr})^2}$. When $i_L$ given by Eq. (10) decreases to zero, the core operation returns to mode I.

The time $t_1$, $t_2$, $t_3$, and $t_4$ satisfy the following equations:

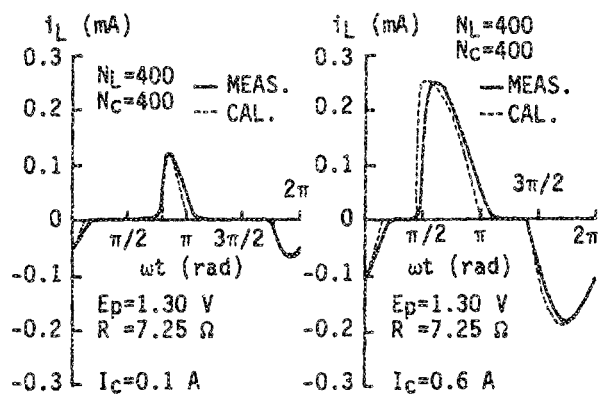


FIG. 5. Comparisons between the calculated output current and measured one.

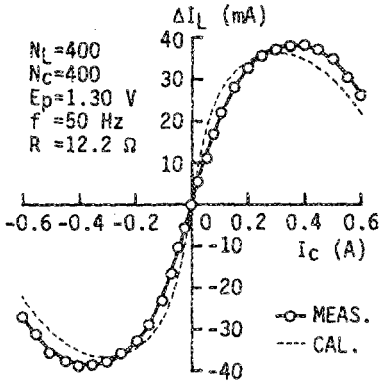


FIG. 6. Relationship between the value $\Delta I_L$ and the dc current $I_C$.

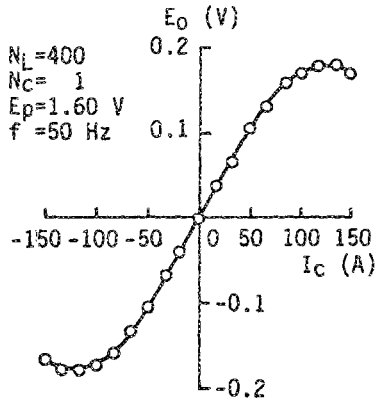


FIG. 8. Relationship between the value $E_0$ and the measuring dc current $I_C$.

$$\cos \omega t_1 - \cos \omega t_2 = (1/\phi_P)(2\Phi_S - P_C N_C I_C),$$
$$\cos \omega t_4 - \cos \omega t_3 = (1/\phi_P)(2\Phi_S - P_C N_C I_C),$$
$$\sin(\omega t_2 - \xi_r)\exp[(t_2 - t_3)/\tau_r] - \sin(\omega t_2 - \xi_r) = 0,$$
$$\sin(\omega t_4 - \xi_{Cr})\exp[(t_4 - t_1 - T)/\tau_{Cr}]$$
$$+ \sin(\omega t_1 - \xi_{Cr}) = 0. \quad (11)$$

Using Eqs. (7), (10), and (11), we can obtain the values of $I_{Lp}$ and $I_{Ln}$.

Figure 5 shows the comparisons of the calculated output current with the experimental one. The following values were used in the calculations: $P_c = 7.60\times10^{-8}$ Wb/A, $P_r = 0.34\times10^{-8}$ Wb/A, and $\Phi_S = 1.42\times10^{-5}$ Wb. From Fig. 5, it is revealed that the calculated values agree well with the experimental ones.

Now, let $\Delta I_L$ denote the difference between positive and negative amplitudes of $i_L$. That is $\Delta I_L = |I_{Lp}| - |I_{Ln}|$.

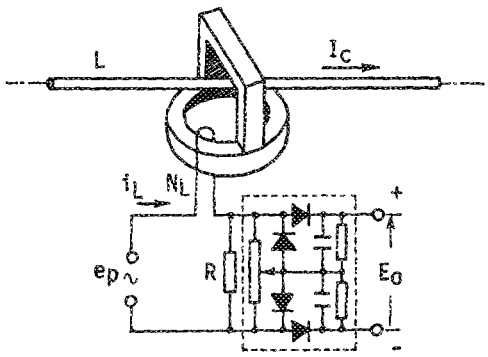


FIG. 7. Circuit configuration of the dc current detector.

Figure 6 shows the relationship between $\Delta I_L$ and the dc current $I_C$. This reveals that $\Delta I_L$ depends on the value and flow direction of the dc current, and that the bridge-connected magnetic circuit is applicable to a dc current detector. If the number of the control winding is one turn, it is expected to measure very large dc current.

## APPLICATION TO A dc CURRENT DETECTOR

Figure 7 shows the circuit configuration of the dc current detector. In the figure, $L$ is the measuring conductor. The voltage $E_0$ of the circuit enclosed with dotted rectangle is proportional to $\Delta I_L$ mentioned above.

Figure 8 shows the relationship between the value $E_0$ and the measuring dc current $I_C$. Good linearity is obtained within the dc current range of $\pm$ 100 A in the experiments.

## CONCLUSION

The operation of a birdge-connected magnetic circuit with single output winding in dc control has been described. The dc current detector presented here can measure a large dc current and detect its flow direction without touching the measuring conductor because the U-form core is easily detached from the toroidal core and clamps on to the measuring conductor.

[1]K. Murakami, T. Watanabe, and A. Goto, IEEE Trans. Magn. **MAG-14**, 966 (1978).
[2]S. Okanuma, O. Ichinokura, and K. Murakami, IEEE Trans. Magn. **MAG-23**, 2773 (1987).
[3]S. Okanuma, O. Ichinokura, and K. Murakami, IEEE Trans. Magn. **MAG-22**, 961, (1986).